Waves in Random and Complex Media

https://www.tandfonline.com/journals/twrm20

Impact factor = 4.853

Accepted November 5th 2022

Computation of Sakiadis flow of an Eyring-Powell rheological fluid from a moving porous surface with a non-Fourier heat flux model

Muhammad Aatif[a], Muhammad Waqas[b,*], O. Anwar Bég[c], Muhammad Zubair[a] and Ali Kadir[c]

[a]Department of Mathematics, Mohi-ud-Din Islamic University Nerian Sharif, Azad Jammu and Kashmir, **Pakistan**

[b]NUTECH School of Applied Sciences and Humanities, National University of Technology, Islamabad, 44000, **Pakistan**

[c]Multi-Physical Engineering Sciences Group (MPESG), Mechanical Engineering Dept., Salford University, School of Science, Engineering and Environment (SEE), Manchester, M54WT, **UK**.

Emails: O.A.Beg@salford.ac.uk (Professor O. Anwar Bég) and A.Kadir@salford.ac.uk (Dr. Ali Kadir)

*Correspondence: muhammadwaqas@nutech.edu.pk (M. Waqas)

ABSTRACT: This article examines theoretically and numerically the effect of non-Fourier heat flux on non-Newtonian (Eyring-Powell) Sakiadis convective flow from a moving permeable surface accompanied by a parallel free-stream velocity, as a simulation of polymeric coating processes. The Cattaneo-Christov model is deployed which features thermal relaxation effects as these are important in thermal polymer processing. The physical flow problem is modelled in a Cartesian coordinate system and the governing conservation differential equations and associated boundary conditions are rendered dimensionless by applying suitable transformations. Liquid velocity and thermal distributions are computed considering numerical procedure namely, a shooting method in conjunction with the 5th order Runge-Kutta algorithm (R-K5) executed in a symbolic software. Validation with the three-stage Lobatto IIIA algorithm in MATLAB is included. The impact of key parameters on streamline distributions is also computed. Velocity is increased with increment in Eyring-Powell first parameter for the Sakiadis case whereas it is reduced with Eyring-Powell second parameter for the case where sheet and liquid are inspiring in the similar direction. The special case of Blasius flow is also examined (stationary sheet). For higher injection, there is a solid dampening in the boundary-layer flow for both Sakiadis and Blasius scenarios. With increment in thermal relaxation parameter and Eyring-Powell first and second parameters, temperatures are strongly reduced, and thermal boundary-layer thickness is suppressed. Higher injection at the wall also depletes temperatures. The Cattaneo-Christov heat

flux model predicts lower temperature and thermal boundary layer thickness due to the thermal relaxation effect than the classical Fourier model. Flow patterns are displayed through 2D and 3D streamline contour plots and non-Newtonian characteristics are also found to exhibit strong modifications in these plots. The computations are useful in industrial high temperature coating flow designs using non-Newtonian materials on a moving substrate.

KEYWORDS: Cattaneo-Christov non-Fourier heat flux; Eyring-Powell non-Newtonian fluid; Moving surface, thermal relaxation; Streamline plots; Runge-Kutta numerical solutions, Thermal polymer coating processes.

1. INTRODUCTION

Heat transfer analysis is fundamental to numerous technological processes including manufacturing of polymers, heat exchanger design, high temperature surface spray deposition, rocket combustion and renewable energy systems (solar and geothermal). This mechanism is encountered in many manufacturing and engineering processes such as nuclear reactor cooling, tribological systems, thermal regulation of electronic devices, gas turbine propulsion, and polymeric materials fabrication. Fourier [1] pioneered the study of thermal conductive heat transfer establishing the parabolic law for heat conduction known as Fourier's law [1]. His work established the basis for modern thermo-mechanics. However, in 1948 Cattaneo [2] refined the Fourier model by taking the effects of thermal relaxation. This non-Fourier model is hyperbolic in nature and achieves the correct behaviour for finite thermal waves in real materials, which is neglected in the classical Fourier model. Heat exchange (transfer) is known to occur due to the temperature difference between different locations. The Cattaneo non-Fourier model overcomes the shortcomings of Fourier's law by determining initial disturbance immediately throughout the whole medium with heat transformation via thermal waves. The heat propagation by means of waves as opposed to diffusion has been explored by numerous researchers. Early investigations in this regard has revealed that this is not merely a low temperature phenomenon but instead it has promising imperative real applications in engineering and modern industrial processes including surface treatment of engineering components, food processing, power generation, skin burn treatment, micro/nanofluidic devices etc. Christov [3] further modified the study of Cattaneo by including Oldroyd's upper convected derivatives to establish a more robust material conventional formulation, leading to the so-called generalized non-Fourier heat transfer model known as the Cattaneo-Christov heat flux model. Straughan [4] analyzed thermal convection in Newtonian liquids with the Cattaneo-Christov model, confirming that thermal relation effects are significant

if the Cattaneo number (which accounts for inertial and length scale effects) is sufficiently large. Tibullo et al. [5] deployed the Cattaneo-Christov heat conduction model for incompressible viscous flow. Abbasi et al. [6] performed an analytical study using the Oldroyd-B rheological model to describe attributes of heat transfer in frames of revised Fourier expression, noting that temperature along with thermal boundary-layer thickness reduce with thermal relaxation aspects, which are overlooked in Fourier model. Further studies utilizing the revised Fourier expression are available in [7 − 8].

Engineering applications of non-Newtonian fluid flows are increasing in the 21st century. Such fluids are encountered in chemical engineering fluidized beds, lubricants, emollients, medical linctus suspensions, sterilizing gels, foams, biotechnological and polymer processing (coatings) etc. Non-Newtonian effects cannot be simulated with the classical Navier-Stokes viscous flow model since it does not feature important phenomena such as couple stresses, stress relaxation, retardation, spurt, viscosity variation, molecular stretching etc. Several constitutive equations of non-Newtonian fluids have therefore been suggested to accurately mimic these characteristics and include the Bingham viscoplastic model, Walters-B viscoelastic model and others [9 − 10]. These models carefully modify the shear-stress behaviour via tensorial formulations to correctly predict non-Newtonian fluid dynamics. Boundary-layer flows of rate type fluids have been in particular investigated utilizing robust constitutive relationships in comparison to the other differential (Reiner-Rivlin) type fluids [11 − 15] . The Eyring-Powell rheological model [16, 17] is an excellent example of a rate type fluid model which is more comprehensive than the conventional Ostwald DeWaele power law model. Although more complex than other non-Newtonian fluid models, since it is derived from kinetic theory of liquids rather than the empirical relation, it has the advantage that it reduces to Newtonian behavior for low and high shear rates. Further, Eyring-Powell model describes shear flows of non-Newtonian fluids, derived from theory of rate processes. It quite accurately describes performance of polymer solutions and viscoelastic suspensions over an extensive range of shear rates [18] .

During various manufacturing processes, flow towards a moving surface is required. In all these procedures thermal treatment of the material traveling over a feed or wind-up roll or assembly line is significant. This scenario features in the fabrication of fibers in glass, polymers transported on conveyor belts, coating dynamics, metallurgical free surface flows, deposition of paints and gels, production of wrapping foils and plastic sheet synthesis. In such processes mass, heat and

momentum transfer play a key role. Polymeric layers may be stretched in specific directions to improve mechanical properties and different thermal loading conditions can be exploited to manipulate final product characteristics. Sakiadis [19] pioneering investigation explored the boundary layer flow with heat transfer over a moving rigid plate (conveyor belt surface). This analysis although confined to Newtonian fluids, established the foundation for modelling boundary layer flows on moving surfaces. Subsequently many researchers examined Sakiadis flows with a wide range of multi-physical effects (thermal radiation, magnetohydrodynamics, wall slip etc). Some relevant articles in this regard are cited in [20 – 23]. Recently, such flows in the presence of free stream velocity effects have been addressed analytically for different viscoelastic polymeric liquids (e.g. Jeffreys and Maxwell fluids) by Hayat et al. [24 – 26] and for the Eyring-Powell model by Zaman et al. [27].

Inspection of the literature has revealed that thus far the Sakiadis flow of an Eyring-Powell polymeric non-Newtonian fluid from a moving surface with non-Fourier heat flux effects, has not been examined. This is the motivation of the present work. A two-dimensional, steady mathematical model is developed using boundary layer theory. The moving surface is porous and accompanied by a parallel free stream velocity. The Cattaneo-Christov model is deployed which features thermal relaxation effects as these are important in thermal polymer processing where a rheological coating material is deposited on a flat translating substrate with complex heat (and mass) transfer (thermal/solutal) effects. This constitutes a key practical application of the current mathematical study. The current work therefore extends the classical Newtonian fluid Sakiadis problem to consider non-Fourier thermal relaxation and Eyring-Powell rheological effects which are shown to modify transport characteristics considerably in the coating flow dynamics studied. The nonlinear transformed dimensionless ordinary differential boundary value problem is solved with a 5^{th} order Runge-Kutta method (R-K5) executed in a symbolic software. Validation with the three-stage Lobatto IIIA algorithm in MATLAB is included. The impact of key parameters on velocity, temperature, skin friction and 3-D streamline distributions is also computed and interpreted in detail.

2. SAKIADIS NON-NEWTONIAN NON-FOURIER FLOW MODEL

Let us formulate the steady-state two-dimensional boundary-layer flow of an incompressible Eyring Powell liquid (shear-thinning polymer) towards moving surface having velocity u_w in the

similar direction as that of uniform free-stream velocity u_∞ . The x-axis is selected along moving surface (i.e., in the direction of motion) and y-axis is in perpendicular direction. The temperature T takes constant value T_w at the moving wall (boundary). Moreover, T_∞ denotes the ambient values of T. It is anticipated that wall and free-stream temperatures T_w and T_∞ are constants with $T_w > T_\infty$. The geometry of the regime is visualized in **Fig. 1**. According to Powell and Eyring [16] , the stress tensor for an Eyring-Powell fluid is:

$$\Lambda = \mu\nabla V + \frac{1}{\beta}\sinh^{-1}\left(\frac{1}{C}\nabla V\right) \tag{1}$$

Here μ is dynamic viscosity, V is fluid velocity, β and C are Eyring-Powell non-Newtonian material parameters. Letting:

$$\sinh^{-1}\left(\frac{1}{C}\nabla V\right) \cong \frac{1}{C}\nabla V - \frac{1}{6}\left(\frac{1}{C}\nabla V\right)^3, \qquad \left|\frac{1}{C}\frac{\partial u_i}{\partial x_j}\right| < 1 \tag{2}$$

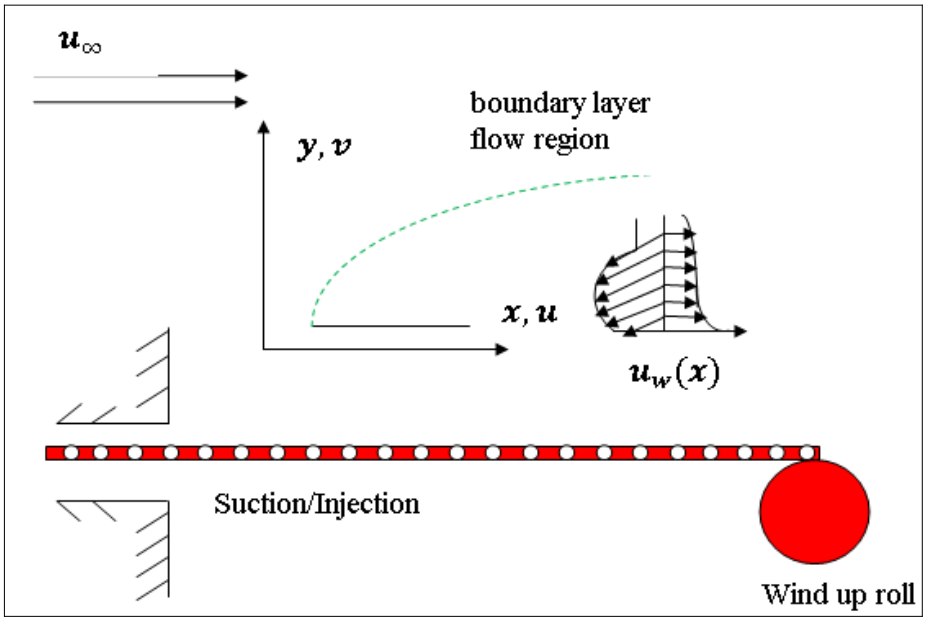

Fig. 1: Physical flow diagram.

Adopting the above relation, the governing boundary-layer equations for considered model are:

$$\frac{\partial u}{\partial x} + \frac{\partial v}{\partial y} = 0 \ , \tag{3}$$

$$u\frac{\partial u}{\partial x}+v\frac{\partial u}{\partial y}=\left(\nu+\frac{1}{\rho\beta C}\right)\frac{\partial^2 u}{\partial y^2}-\frac{1}{2\rho\beta C^3}\left(\frac{\partial u}{\partial y}\right)^2\frac{\partial^2 u}{\partial y^2}\ , \tag{4}$$

The prescribed boundary conditions at wall and in the free-stream are:

$$u=u_w(x)\,,\qquad v=v_w\qquad at\qquad y=0\,,$$
$$u\to u_\infty(x),\qquad \frac{\partial u}{\partial y}\to 0\qquad as\qquad y\to\infty \tag{5}$$

in which ρ is denoted by density, u and v are velocity components along x and y directions respectively and ν is liquid's kinematic viscosity. In addition, the non-Fourier (Cattaneo-Christov) heat flux model (see Cattaneo [2] and Christov [3]) can be expressed as follows:

$$q+\lambda_3\left(\frac{\partial q}{\partial t}+V.\nabla_q-q.\nabla V-(\nabla.V)_q\right)=-k\nabla T\ , \tag{6}$$

Here q is the heat flux, λ_3 is the relaxation time for heat flux, k is the thermal conductivity and V is the velocity vector. In view of the above expression, the energy equation is modified to:

$$u\frac{\partial T}{\partial x}+v\frac{\partial T}{\partial y}+\lambda_3\begin{pmatrix} u\frac{\partial u}{\partial x}\frac{\partial T}{\partial x}+v\frac{\partial v}{\partial y}\frac{\partial T}{\partial y}+u\frac{\partial v}{\partial x}\frac{\partial T}{\partial y} \\ +v\frac{\partial u}{\partial y}\frac{\partial T}{\partial x}+2uv\frac{\partial^2 T}{\partial x\,\partial y}+u^2\frac{\partial^2 T}{\partial x^2}+v^2\frac{\partial^2 T}{\partial y^2}\end{pmatrix}=\alpha\frac{\partial^2 T}{\partial y^2} \tag{7}$$

The associated thermal boundary conditions are:

$$T=T_w(x)\qquad at\qquad y=0;\qquad T\to T_\infty\qquad as\qquad y\to\infty \tag{8}$$

In Eqns. (7) and (8), α is thermal diffusivity, T_w is temperature at the wall, and T_∞ is the ambient fluid temperature. To proceed further, we introduce following dimensionless quantities:

$$u=Uf'(\eta),\quad v=-\frac{1}{2}\sqrt{\frac{U\nu}{x}}[f(\eta)-\eta f'(\eta)]\,,\quad \eta=y\sqrt{\frac{U}{x\nu}}\ ,\quad \theta(\eta)=\frac{T-T_\infty}{T_w-T_\infty} \tag{9}$$

Here $U=u_w+u_\infty$. In view of Eqn. (9), Eqn. (1) is automatically fulfilled and other Eqns. (2), (3), (7) and (8) are reduced into following coupled momentum and thermal boundary layer equations:

$$(1+\epsilon)f''' + \frac{1}{2}ff'' - \epsilon\delta(f'')^2 f''' = 0 \tag{10}$$

$$\theta'' + \frac{1}{2}\Pr f\theta' - \frac{\Pr\gamma}{4}(3ff'\theta' + f^2\theta'') = 0 \tag{11}$$

$$\begin{aligned} &f'(\eta) = \lambda, \quad f(\eta) = S, \quad \theta(\eta) = 1 \quad \text{at} \quad \eta = 0 \\ &f'(\eta) = 1-\lambda, \quad \theta(\eta) = 0 \quad \text{as} \quad \eta \to \infty \end{aligned} \tag{12}$$

Here $f(0) = S$ with $S < 0$ corresponding to the suction case and $S > 0$ implying injection (blowing), λ is a parameter relating the wall velocity to free stream velocity, Pr is the Prandtl number, ϵ and δ are Eyring-Powell non-Newtonian material parameters and γ is the non-Fourier relaxation time (Cattaneo-Christov parameter). These dimensionless physical parameters take the following definitions:

$$\begin{aligned} &\lambda = \frac{u_w}{U}, \quad \Pr = \frac{\nu}{\alpha}, \quad \delta = \frac{U^3}{2xvC^2}, \\ &\gamma = \frac{\lambda_3 U}{x}, \quad \epsilon = \frac{1}{\mu\beta C}, \quad S = -\left(\sqrt{\frac{2x}{\nu U}}\right)v_w \end{aligned} \tag{13}$$

Here it is worth-mentioning that $\lambda = 0$ yields the flow by stationary surface induced by free-stream velocity (i.e., Blasius flow). The case, $\lambda = 1$ yields moving wall (Sakiadis flow). The situation $0 < \lambda < 1$ is when fluid and wall are persuading in the similar direction. Moreover, if $\lambda > 1$, the free-stream is directed towards the negative x - direction while the wall moves in positive x - direction. In materials processing operations, an important physical quantity (i.e., kin friction coefficient C_f) which is delineated as:

$$C_f = \frac{\tau_w}{\rho U^2} \tag{14}$$

In dimensionless form, one obtains the skin friction as:

$$-\mathrm{Re}_x^{\frac{1}{2}} C_f = (1+\epsilon)f''(0) - \frac{\epsilon}{3}\delta f''^3(0) \tag{15}$$

Where $\mathrm{Re}_x = \frac{U_x}{\nu}$ is the local Reynolds number.

3. RUNGE-KUTTA NUMERICAL SOLUTIONS

This section describes the numerical solution of the governing Eqns. (10) and (11) subject to

boundary conditions (12) via the deployment of a shooting algorithm along with the 5th order Runge Kutta quadrature method (R-K-5). For this purpose, the nonlinear ordinary differential equations (10) and (11) are converted into a first order equations as an initial value problem and the variables are defined as follows:

$$(f, f', f'', \theta, \theta')^{T} = (y_1,\ y_1' = y_2, y_2' = y_3, y_4, y_4' = y_5)^{T} \tag{16}$$

In view of above substitutions, the initial value problem can be defined as:

$$\begin{pmatrix} y_1' \\ y_2' \\ y_3' \\ y_4' \\ y_5' \end{pmatrix} = \begin{pmatrix} y_2 \\ y_3 \\ \dfrac{-(1/2) y_1 y_3}{(1+\epsilon-\epsilon\delta(y_3)^2)} \\ y_5 \\ \dfrac{(3/4)\mathrm{Pr}\gamma y_1 y_2 y_5 - (1/2)\mathrm{Pr} y_1 y_4}{(1-(1/4)\mathrm{Pr}\gamma(y_1)^2)} \end{pmatrix}$$

$$\begin{pmatrix} y_1(0) \\ y_2(0) \\ y_3(0) \\ y_4(0) \\ y_5(0) \end{pmatrix} = \begin{pmatrix} S \\ \lambda \\ U_1 \\ 1 \\ U_2 \end{pmatrix} \tag{17}$$

Apposite estimations of unknown conditions (U_1 and U_2) are approximated via Newton's scheme until the boundary conditions ($f'(\eta) \to 1-\lambda$, and $\theta(\eta) \to 0$ as $\eta \to \infty$) are satisfied.

4. VALIDATION WITH MATLAB BVP5C THREE-STAGE LOBATTO IIIA SOLVER

We adopted the three-stage formula (Lobatto IIIA) to validate the RK-5 numerical shooting solutions. The mesh size along with error control are reliant on the residue of continuous solution acquired from collocation polynomial which utilizes the fourth-order precision in interval [a, b]. The technique followed is that non-linear differential systems are written again in first-order differential equations. The said numerical solver possessed eight decimal places of order. The successful execution of code saves the mesh data in sol. x, while the numerical results are saved in sol. y. This technique has been employed in a variety of nonlinear complex fluid dynamics problems including Bég et al. [28], Uddin et al. [29] and Sarkar and Sahoo [30]. Bvp5c is

implemented to compute the value of Y_{MID} along with gradient at the ends of subinterval. The formula used to calculate Y_{MID} is:

$$Y_{MID} = Y_1 + \zeta\left[\frac{17}{192}K_1 + \frac{40+15\sqrt{5}}{192}K_2 + \frac{40+15\sqrt{5}}{192}K_3 - \frac{1}{192}K_4\right] \quad (18)$$

Here Y_1 is the initial guess and K_1, K_2, K_3, K_4 are the estimates having stepping distance ζ. Exceptional stable solutions are obtained. Table 1 shows comparison of $-\mathrm{Re}_x^{\frac{1}{2}}C_f$ for $\lambda = 1$ i.e. Sakiadis flow and Blasius flow ($\lambda = 0.2$). Excellent correlation is achieved testifying to the accuracy of the R-K-5 numerical solutions. Computational values are displayed up to four decimal places. From this table it is also evident that for the case of Sakiadis flow i.e. $\lambda = 1$, coefficient of skin friction is enhanced for rising values of ϵ i. e. Eyring-Powell first non-Newtonian material parameter and S (wall injection) whereas it is decreased with increment in the Eyring-Powell second non-Newtonian material parameter (δ). The different response in skin friction with different Eyring-Powell parameters is due to the different nature of the shear terms in which they appear in the momentum Eqn. (10).

Table 1: Comparison of R-K and MATLAB BVP5C solutions for wall skin friction with different model parameters.

ϵ	δ	S	$-\mathrm{Re}_x^{\frac{1}{2}}C_f$ ($\lambda = 1$) Sakiadis flow R-K scheme	$-\mathrm{Re}_x^{\frac{1}{2}}C_f$ ($\lambda = 1$) Sakiadis flow [MATLAB three-stage Lobatto IIIA]	$-\mathrm{Re}_x^{\frac{1}{2}}C_f$ ($\lambda = 0.2$) Blasius flow R-K Scheme	$-\mathrm{Re}_x^{\frac{1}{2}}C_f$ ($\lambda = 1$) Blasius flow [MATLAB three-stage Lobatto IIIA]
1.0	0.1	2.5	1.5519	1.5522	−0.9105	−0.9102
2.0			1.6670	1.6672	−0.9676	−0.9673
3.0			1.7714	1.7717	−1.0179	−1.0175
4.0			1.8694	1.8693	−1.0639	−1.0636
1.5	0.3		1.6083	1.6086	−0.9398	−0.9392
	0.5		1.6054	1.6056	−0.9395	−0.9391
	0.7		1.6023	1.6027	−0.9392	−0.9397
	0.9		1.5989	1.5993	−0.9389	−0.9384
	0.5	0.0	0.7024	0.7028	−0.3435	−0.3432
		0.5	0.8567	0.8570	−0.4499	−0.4493
		1.0	1.0260	1.0264	−0.5642	−0.5648
		1.5	1.2085	1.2088	−0.6847	−0.6841

The first parameter features in the momentum assisting term, $(1+\epsilon)f'''$, producing strong acceleration i. e. larger skin friction coefficient and a thicker momentum boundary layer. However, the second parameter is attached to the negative shear term, $-\epsilon\delta(f'')^2f'''$ leading to strong deceleration i. e. lower skin friction coefficient. Momentum boundary layer thickness is therefore increased. Injection clearly exacerbates the lateral mass flux through the wall and aids the boundary layer flow, inducing strong acceleration and larger skin friction coefficient. A very different response is observed for the classical Blasius flow (stationary wall, $\lambda = 0.2$). Here skin friction is decreased i. e. values are more negative with increment in Eyring-Powell first non-Newtonian material parameter (ϵ) and injection parameter (S) whereas it is now enhanced (less negative values) with Eyring-Powell second non-Newtonian material parameter (δ). The negative values of skin friction imply back flow i. e. flow reversal. In the next section all figures are based on the R-K-4 numerical method results.

5.GRAPHICAL RESULTS AND DISCUSSION

In this section, R-K-5 numerical results are displayed through graphs and tables. Graphs are designed to explore the influence of pertinent parameters i.e. velocity ratio, λ , Eyring-Powell first and second non-Newtonian material fluid parameters (ϵ and δ), suction/injection parameter S , Prandtl number Pr and non-Fourier thermal relaxation parameter, γ on thermo-fluid characteristics. Figures 2 to 8 are plotted for velocity distribution for various selected parameters. Here $\lambda = 1$ depicts the Sakiadis flow case while $0 \leq \lambda < 1$ demonstrates the Blasius flow case. Figure 2 is plotted for $f'(\eta)$ against η for significant values of λ by keeping ϵ , δ and S fixed. It is evident that for $0 \leq \lambda \leq 0.2$, liquid velocity is enhanced (acceleration) in the neighborhood of moving surface (i.e., momentum boundary-layer thickness is decreased) while subsequently it is a decreasing function of λ, (i.e., momentum boundary-layer thickness is augmented due to flow retardation) and this trend is continued into the free-stream. Asymptotically smooth results are computed at the maximum value of the transverse coordinate (η) i. e. in the free-stream, ratifying the prescription of an sufficiently large infinity boundary condition in the R-K-5 computations.

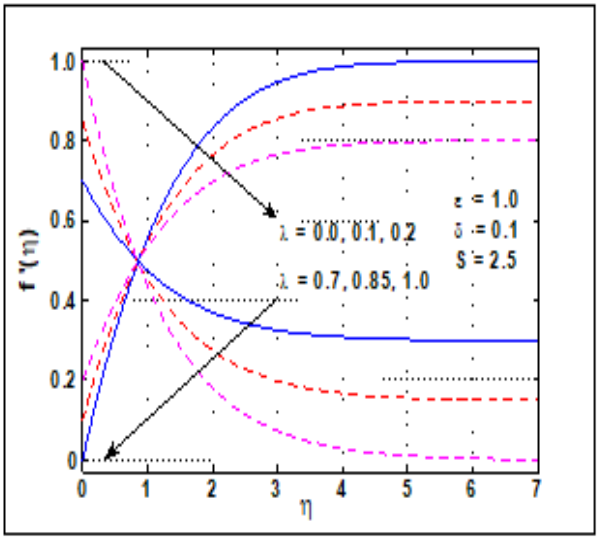

Fig. 2: Influence of λ on $f'(\eta)$.

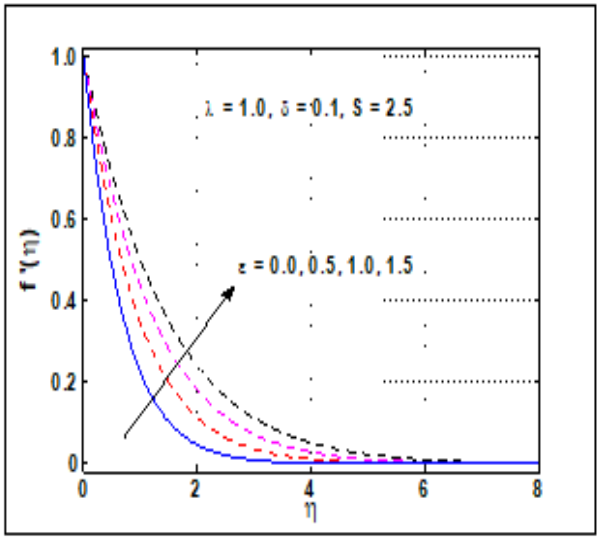

Fig. 3: Influence of ϵ on $f'(\eta)$ when $\lambda = 1.0$

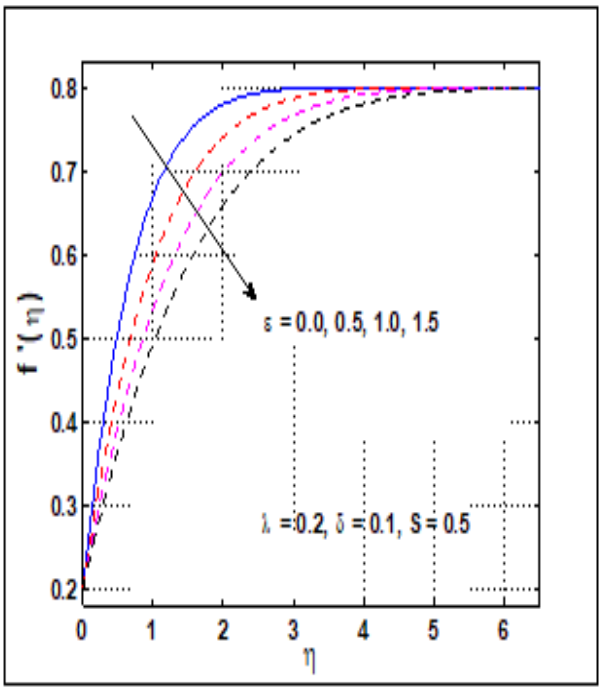

Fig. 4: Influence of ϵ on $f'(\eta)$ when $\lambda = 0.2$

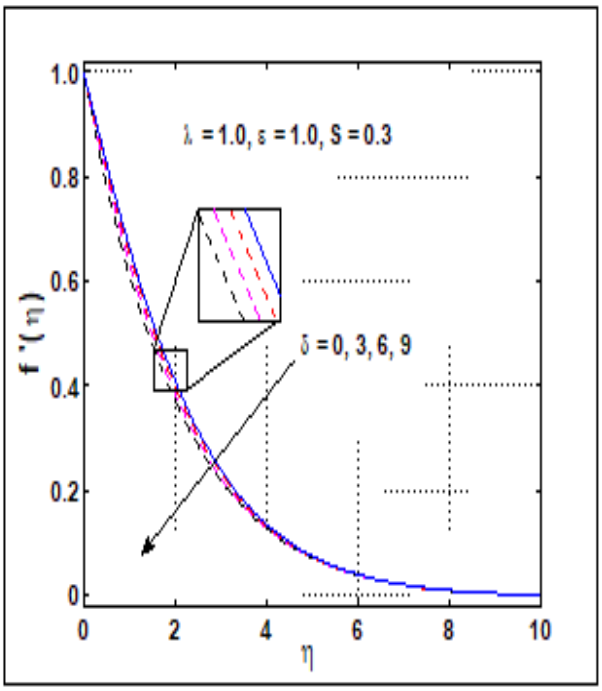

Fig. 5: Influence of δ on $f'(\eta)$ when $\lambda = 1.0$

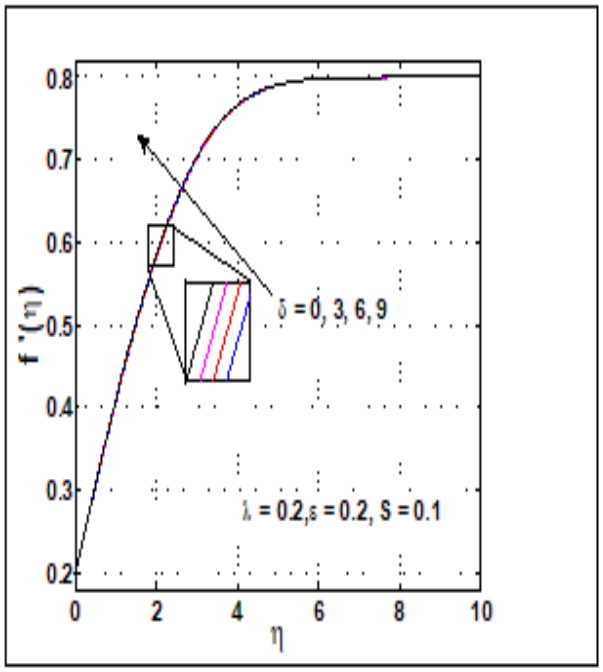

Fig. 6: Influence of δ on $f'(\eta)$ when $\lambda = 0.2$

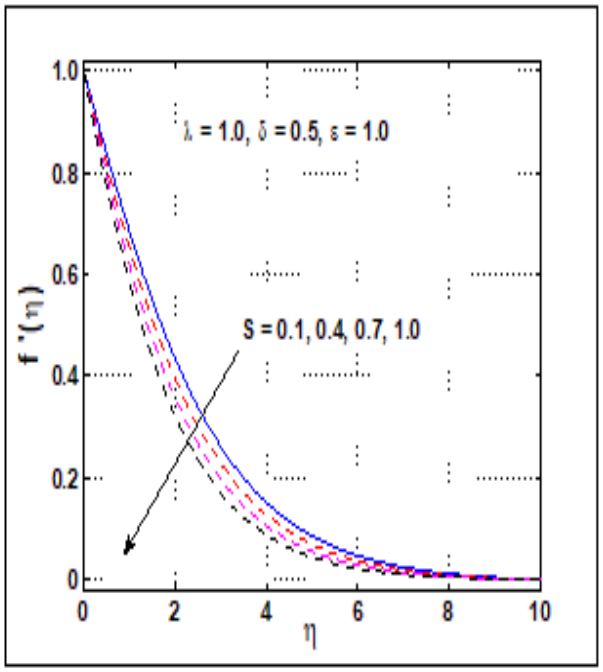

Fig. 7: Influence of S on $f'(\eta)$ when $\lambda = 1.0$

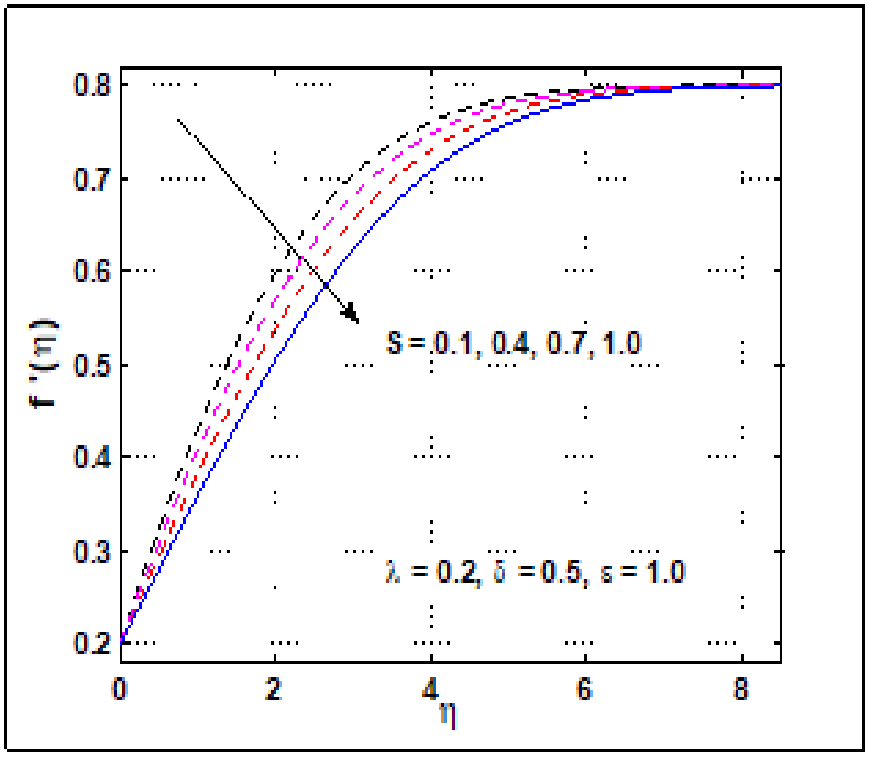

Fig. 8: Influence of S on $f'(\eta)$ when $\lambda = 0.2$

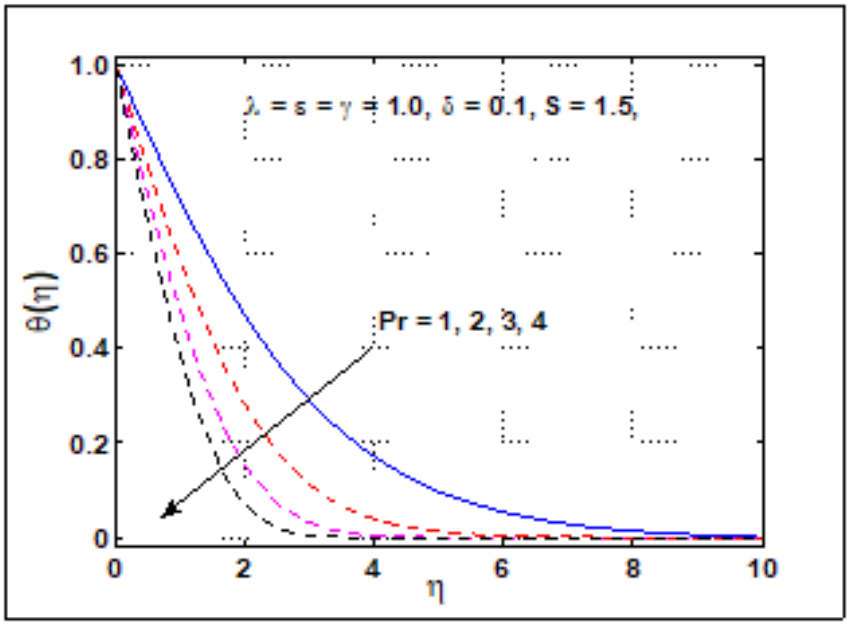

Fig. 9: Influence of Pr on θ(η)

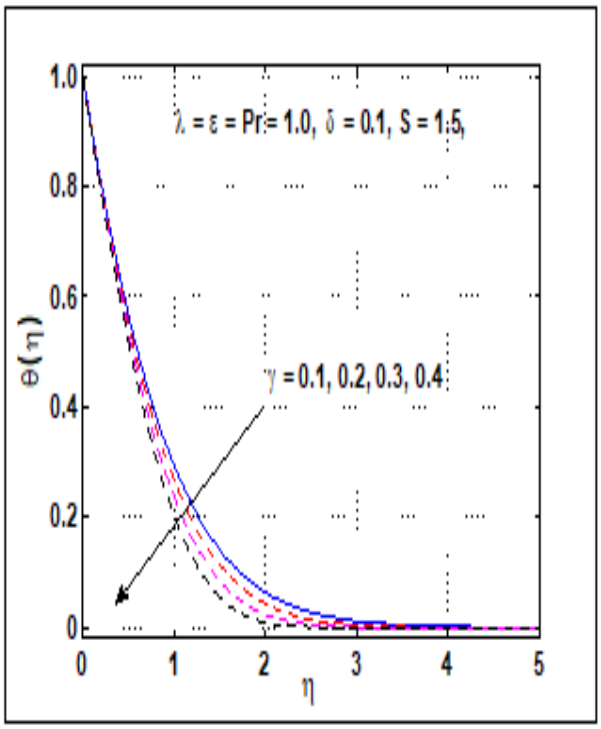

Fig. 10: Influence of γ on θ(η)

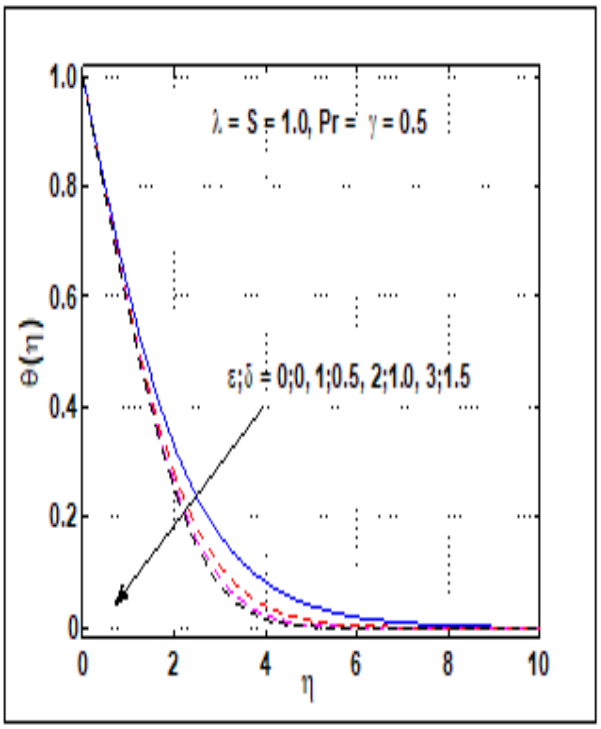

Fig. 11: Influence of ε and δ on θ(η)

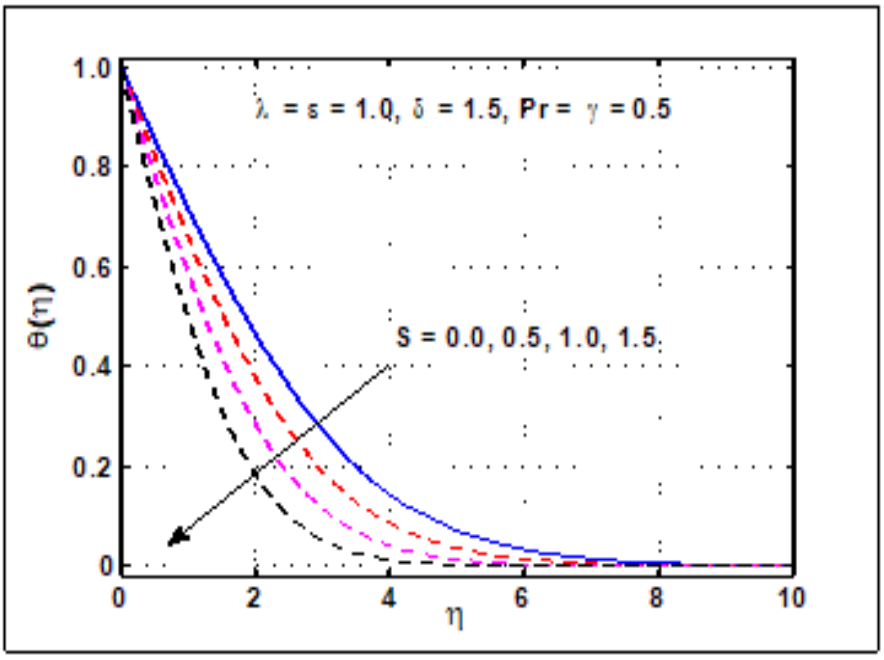

Fig. 12: Influence of S on $\theta(\eta)$

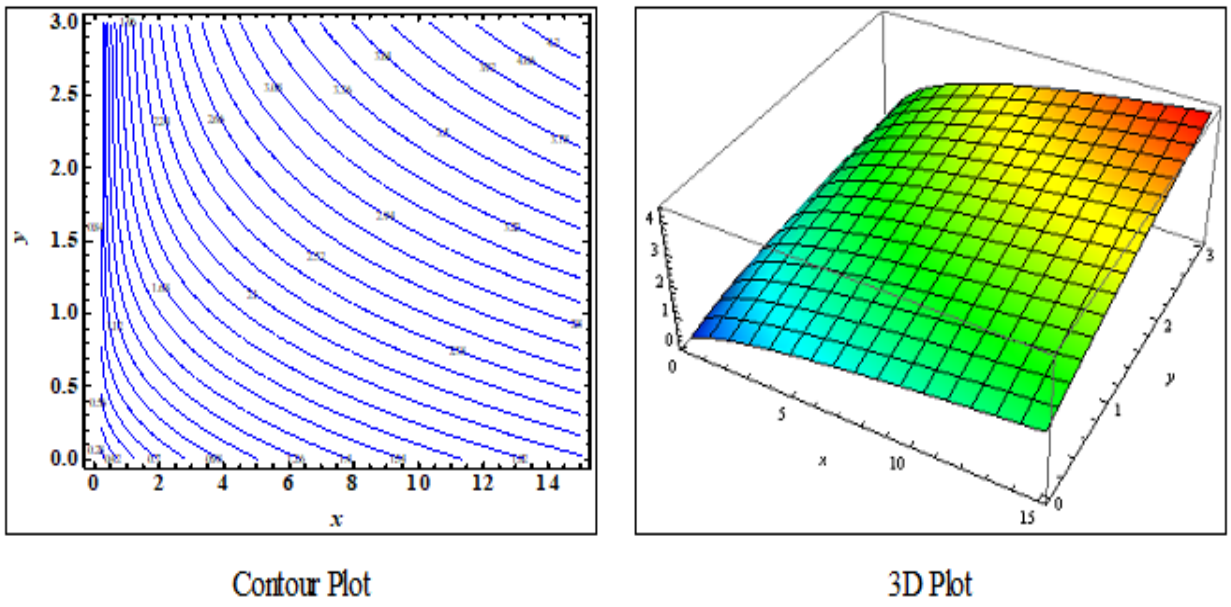

Fig. 13: Streamlines for Sakiadis flow when $\epsilon = 0.2$

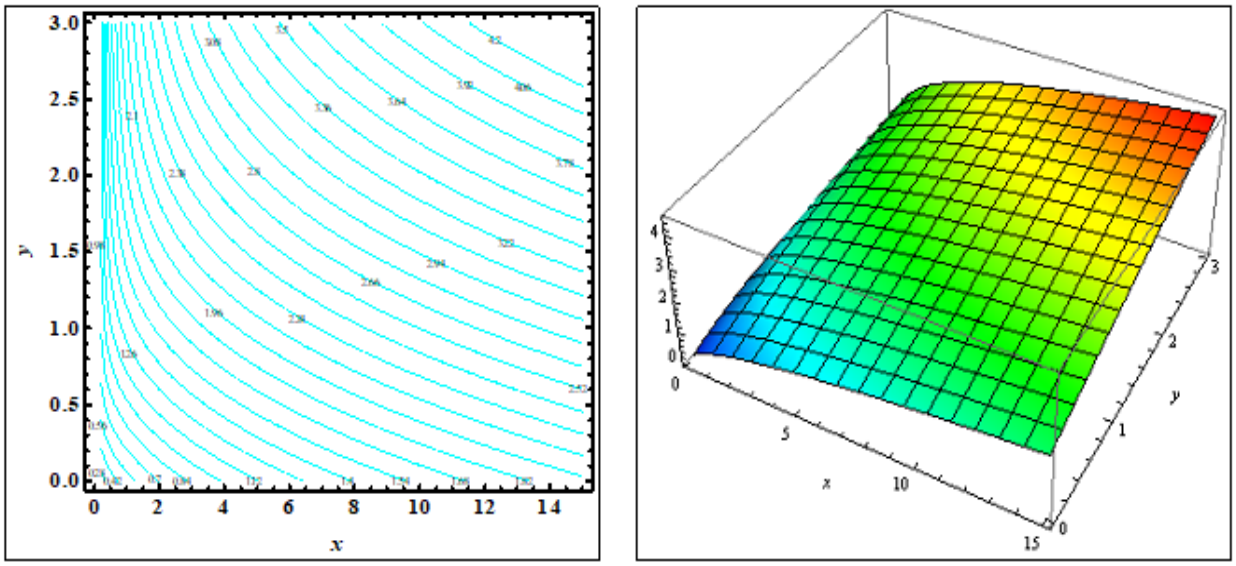

Contour Plot 3D Plot

Fig. 14: Streamlines for Sakiadis flow when $\epsilon = 1.0$

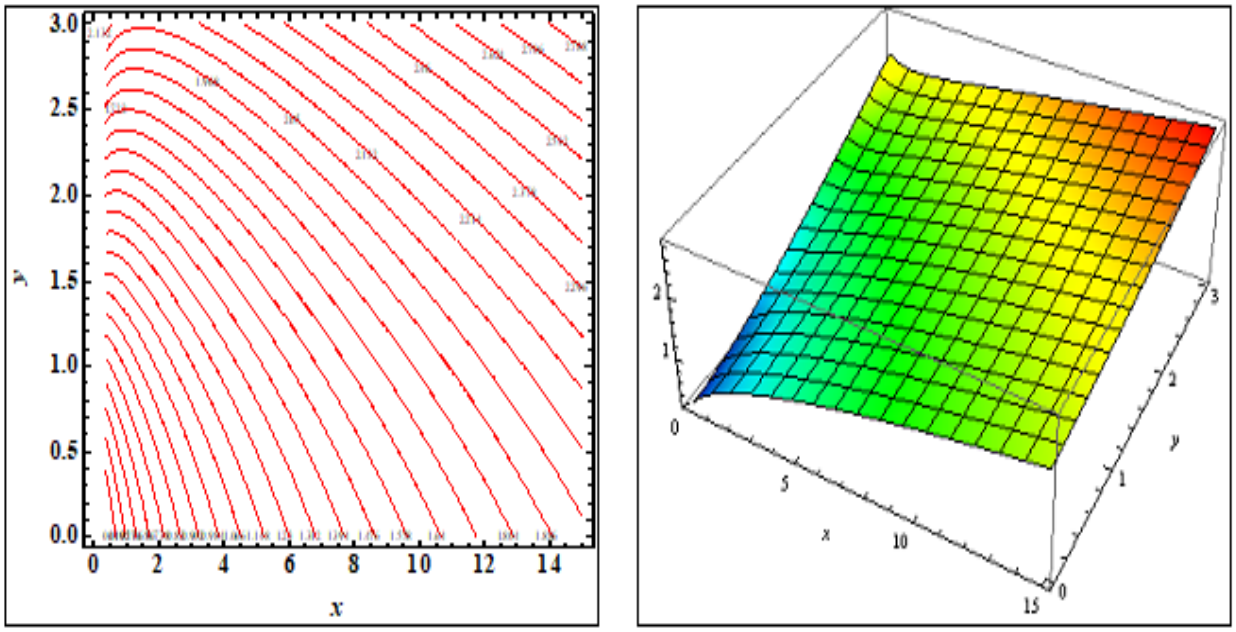

Contour Plot 3D Plot

Fig. 15: Streamlines for Blasius flow when $\epsilon = 0.2$.

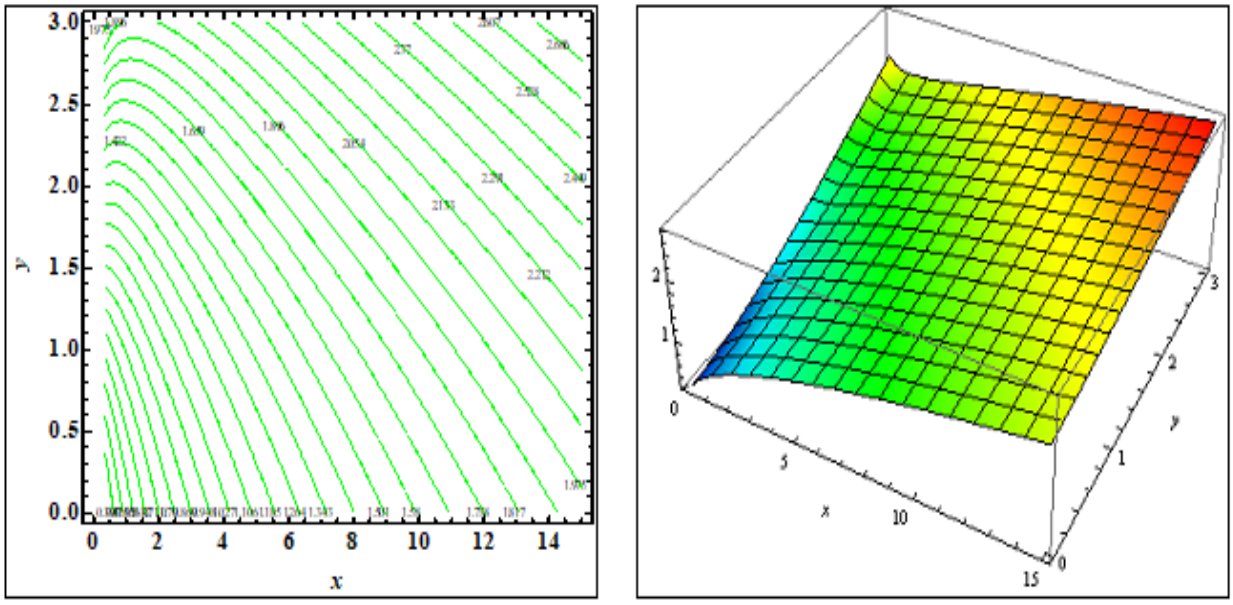

Contour Plot 3D Plot

Fig. 16: Streamlines for Blasius flow when $\epsilon = 1.0$

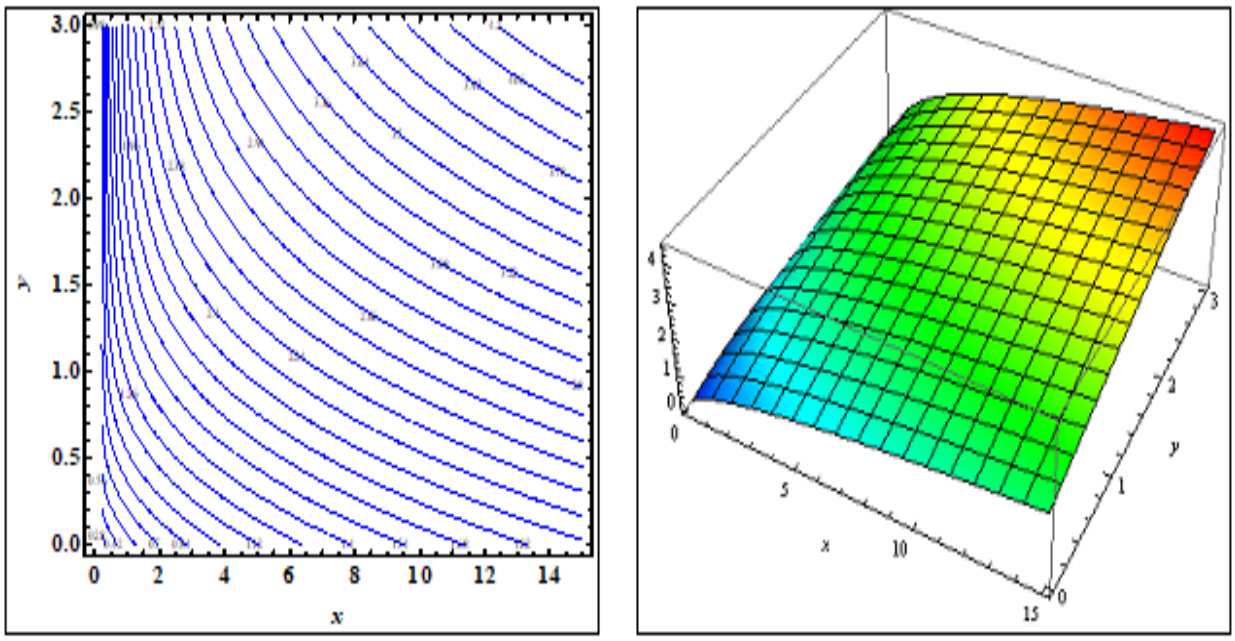

Contour Plot 3D Plot

Fig. 17: Streamlines for Sakiadis flow when $\delta = 1.0$

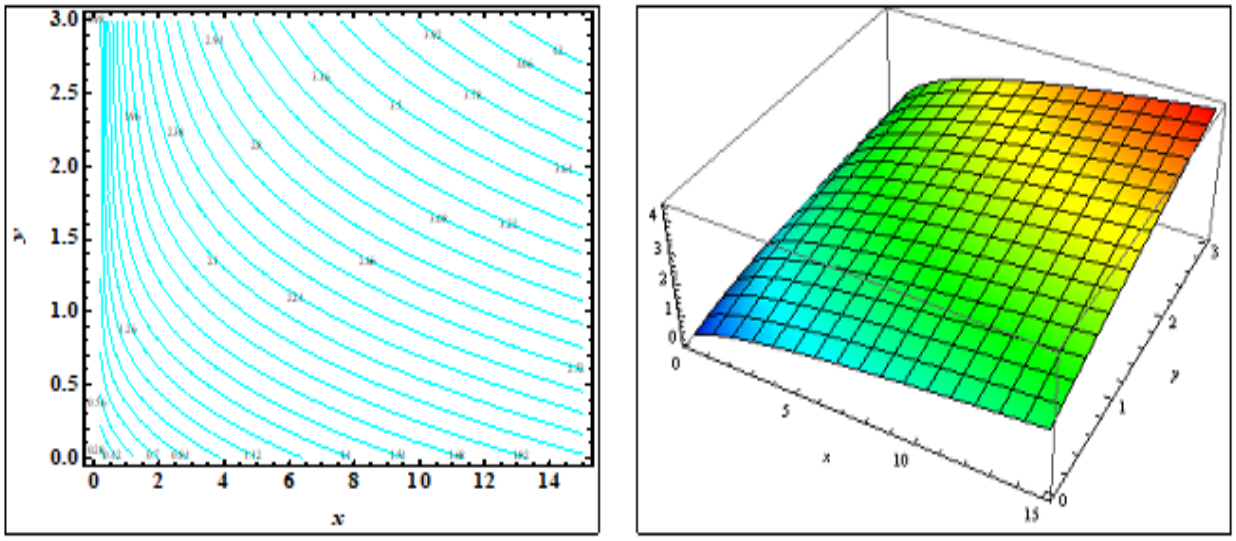

Fig. 18: Streamlines for Sakiadis flow when $\delta = 3.0$.

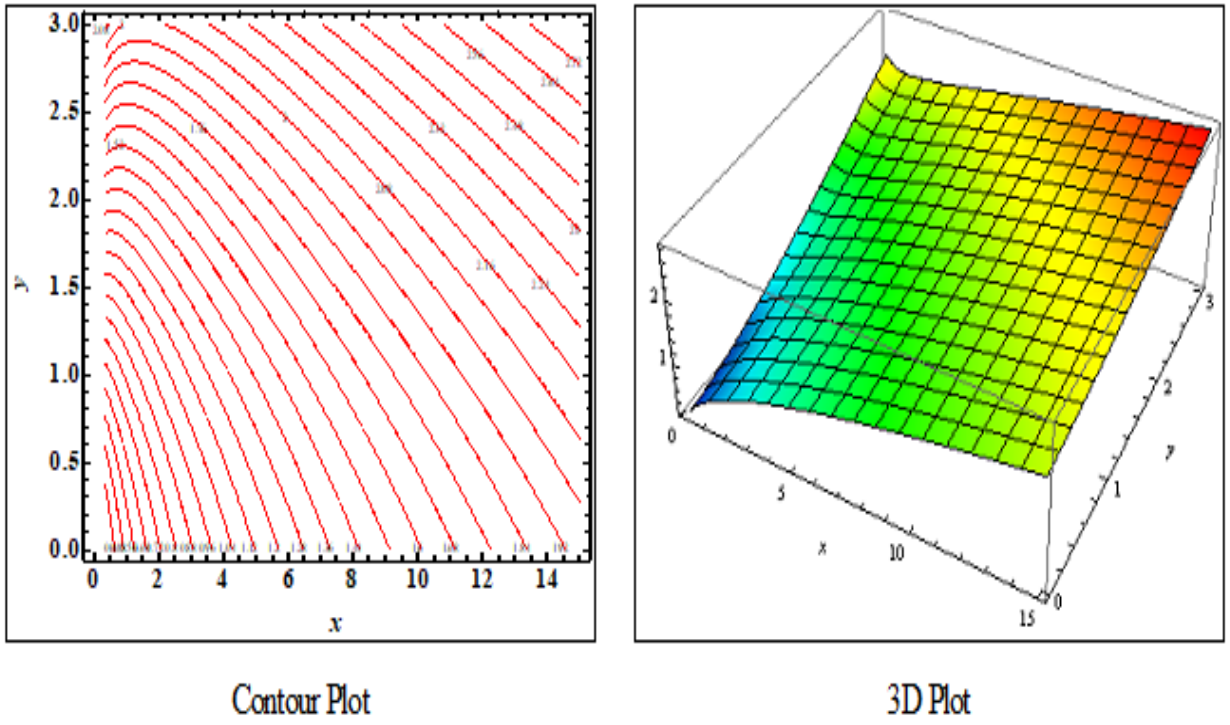

Fig. 19: Streamlines for Blasius flow when $\delta = 1.0$.

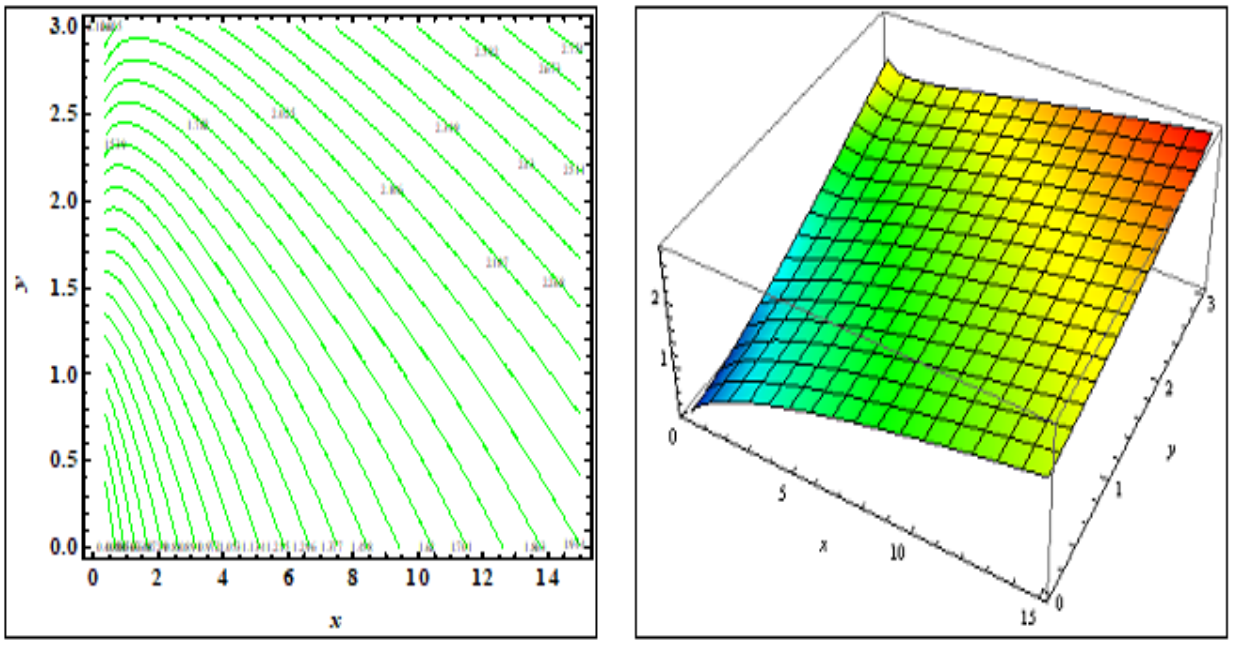

Fig. 20: Streamlines for Blasius flow when $\delta = 3.0$

Figures 3 and 5 illustrate the effect of fluid property parameter ϵ and δ for the Sakiadis flow (λ=1.0). It is noted, that greater ϵ contributes towards accelerating the fluid flow whereas increment in in δ produces deceleration, and as noted this is due to the assistive shear term for the former parameter and the negative shear term for the latter parameter in the momentum boundary layer eqn. (10). It is also noteworthy that $\epsilon = \frac{1}{\mu\beta C}$ which indicates that it is inversely proportional to dynamic viscosity and thus, an increase in ϵ leads to a reduction in low resistance and hence acceleration and a thinner momentum boundary layer thickness (see figure 3). δ is inversely related to streamwise coordinate, x. Thus, an increase in δ implies a decrease in sheet length which contributes to inhibited space for the boundary layer growth and results in deceleration and a thicker boundary layer thickness (see figure 5). The opposite behavior is observed for the case of Blasius flow (see figures 4 and 6) for the two fluid parameters. Therefore, the presence of a moving wall (Sakiadis flow) has a dramatic influence on the impact of Eyring-Powell non-Newtonian parameters on momentum characteristics. The effects of wall injection, $S > 0$ for Sakiadis and Blasius flows are displayed in figures 7 and 8, respectively. In case of Sakiadis flow (Fig. 7) the polymer fluid flow is decelerated with greater wall injection (blowing) and the

hydrodynamic (momentum) boundary layer thickness increases. A similar trend is also computed in the case of Blasius flow (stationary wall) where the lateral mass flux introduced into the regime via the wall (injection) again results in strong flow deceleration and a thickening in momentum boundary layer thickness, as seen in figure 8. However, it is evident that the profile topologies are very different. The maximum velocity is computed at the wall with Sakiadis flow (fig. 7) and profiles follow a monotonic decay from the wall to the free stream. However, in Blasius flow, the profiles grow monotonically from the wall to attain a maximum value in the free-tream (edge of the boundary layer). In both cases again asymptotically smooth distributions are attained in the free-stream, verifying that a adequately larger infinity boundary condition has been used in R-K-5 computations.

The impact of key parameters on temperature distributions are visualized in Figures 9 to 12 for Sakiadis flow i. e. $\lambda = 1$. Fig. 9 shows that elevation in Prandtl number induces a strong depletion in temperature, $\theta(\eta)$. Higher values of Prandtl number (Pr =4) correspond to low density polymeric suspensions [31]. Prandtl number signifies the ratio of viscous to thermal diffusion rate. It is also contrariwise proportional to thermal conductivity. Higher Prandtl number (e.g. polymers) correspond to much lower thermal conductivities and this inhibits thermal diffusion leading to reduction in temperature and decrease in thermal boundary layer thickness. A strong monotonic decay in temperature is witnessed from the wall to the free stream at any value of Prandtl number. Fig. 10 shows the influence of thermal relaxation (non-Fourier) parameter on temperature evolution. $\gamma = \frac{\lambda_3 U}{x}$ and features in the augmented convective heat transfer terms, $-\frac{Pr\gamma}{4}(3ff'\theta' + f^2\theta'')$ in Eqn. (11). The Fourier classical case is retrieved when γ =0 for which the thermal boundary layer Eqn. (11) reduces to the classical Prandtl version. With increment in γ thermal waves are intensified in the regime due to the hyperbolicity of the non-Fourier model. This inhibits thermal diffusion and suppresses temperature and also decreases thermal boundary layer thickness Effectively the Fourier model therefore over-predicts temperatures and much better accuracy is achieved with the non-Fourier (Cattaneo-Christov) heat flux approach. This is of particular interest in polymeric coating flows where properties of finished products e. g. coatings are very sensitive to temperature differences, as noted by Gaffar et al. [32]. Overall, it is observed that temperature along with thermal boundary-layer thickness are less in the case of revised Fourier model in comparison to classical Fourier heat-flux model. Figure 11 shows that a noticeable decrement in temperature $\theta(\eta)$ accompanies a rise in both first (ϵ) and second (δ) Eyring-Powell

rheological material parameters. Both parameters, $\epsilon = \frac{1}{\mu\beta C}$ and $\delta = \frac{U^3}{2xvC^2}$ are inversely proportional to the polymer viscosity. This decreases the resistance to flow. Although these rheological parameters only arise in the momentum Eqn. (10), via the terms, $+\frac{1}{2}\Pr f\theta', -\frac{Pr\gamma}{4}(3ff'\theta' + f^2\theta'')$ in the energy Eqn. (11) there is a strong coupling between velocity and temperature fields. Temperature is therefore indirectly influenced by the polymer rheology and therefore thermal boundary layer thickness is effectively reduced with increment in (ϵ) and (δ). Fig 12 displays that with increasing wall injection there is a significant decrease in temperatures in the boundary layer. The case of a solid wall (S = 0) achieves the maximum temperature. Injection therefore serves to cool the boundary layer regime and depletes thermal boundary layer thickness.

Figures $13 - 20$ illustrate the 2-dimensional streamline contour plot (flow pattern) and 3-D plots for different values of ϵ and δ for both Sakiadis ($\lambda = 1$) as well as Blasius flows ($\lambda < 1$), respectively. It is evident that when $\epsilon = 0.2$, i.e. the weakly non-Newtonian case, the flow pattern for Sakiadis flow is concave downwards (see Fig. 13 and 14) while it is concave upwards in Blasius flow when $\epsilon = 1.0$ i.e. for the strongly non-Newtonian case (see Fig. 15 and 16). Furthermore when $\delta = 1.0$ (again weakly non-Newtonian case) the streamline flow pattern for Sakiadis flow faces downwards (see Fig. 17 and 18) while it is directed upwards in Blasius flow when $\delta = 3.0$ (see Fig. 19 and 20). Effectively the combination of non-Newtonian characteristics as simulated via the Eyring-Powell model and the nature of the regime (moving wall or stationary wall) have a dramatic influence on the patterns of flow in the boundary layer.

6. CONCLUSIONS

Motivated by rheological thermal flow processing applications (e.g. coating dynamics) a theoretical and computational study has been described to evaluate the effects of non-Fourier heat flux on non-Newtonian (Eyring-Powell) Sakiadis convective flow from a moving porous surface accompanied by a parallel free stream velocity. The Cattaneo-Christov hyperbolic heat flux model is deployed which features thermal relaxation effects. The transformed dimensionless boundary value problem is solved numerically with a shooting method in conjunction with the 5^{th} order Runge-Kutta method (R-K5) executed in a symbolic software. Validation with the three-stage Lobatto IIIA algorithm in MATLAB software is included. The impact of key parameters on

velocity, temperature, skin friction and streamline distributions is computed. The principal findings of the current study may be summarized as follows:

(i) Flow acceleration is induced with increment in Eyring-Powell first parameter for the Sakiadis case whereas flow deceleration is produced with increment in Eyring-Powell second parameter for Blasius flow (stationary wall).

(ii) With increasing wall injection there is a strong dampening in the boundary layer flow for both Sakiadis and Blasius flow cases.

(iii) With increment in thermal relaxation parameter and Eyring-Powell first and second parameters, temperatures are strongly reduced, and thermal boundary layer thickness is suppressed.

(iv) Greater injection at the wall depletes temperatures and decreases thermal boundary layer thickness.

(v)The Cattaneo-Christov heat flux model predicts lower temperature and thermal boundary layer thickness due to the thermal relaxation effect than the classical Fourier model.

(vi) For the case of Sakiadis flow, skin friction is enhanced with greater values of Eyring-Powell first non-Newtonian material parameter and wall injection whereas it is decreased with increment in the Eyring-Powell second non-Newtonian material parameter.

(vii) 2-D and 3-D streamline contour plots reveal that for the weakly non-Newtonian case, the flow pattern for Sakiadis flow is concave downwards while it is concave upwards in Blasius flow for the strongly non-Newtonian case.

The present computations reveal some further insights into thermal polymer coating flows. However, in the current model mass transfer i. e. species diffusion [33] has been neglected. This may be considered in future studies.

REFERENCES

[1] Fourier, J.B.J. Theorie Analytique De La Chaleur, Chez Firmin Didot, Paris, 1822.

[2] Cattaneo, C. Sullaconduzion edelcalore, in: Atti del Seminario Matematico e Fisico dell Universita di Modena e Reggio Emilia, 3, $83-101$ (1948)

[3] Christov, C.I. On frame in different formulation of the Maxwell-Cattaneo model of finite-speed heat conduction, Mech. Res. Commun. 36, $481-486$ (2009)

[4] Straughan, B. Thermal convection with the Cattaneo-Christov model, Int. J. Heat Mass Transf.

53, 95 – 98 (2010)

[5] Tibullo, V., and Zampoli, V.A uniqueness result for the Cattaneo-Christov heat conduction model applied to incompressible fluids, Mech. Res. Commun. 38, 77 – 79 (2011)

[6] Abbasi, F.M., Mustafa, M., Shehzad, S.A., Alhuthali, M.S., and Hayat, T. Analytical study of Cattaneo-Christov heat flux model for a boundary layer flow of Oldroyd-B fluid, Chin. Phys. B, 25, 014701 (2015)

[7] Mishra, S.R., Shamshuddin, M., Bég, O.A., and Kadir, A. Numerical study of heat transfer and viscous flow in a dual rotating extendable disk system with a non-Fourier heat flux model, Heat Transfer, 48 (1), 435-459 (2019).

[8] Kumaran, G., Sivaraj, R., Prasad, V.R., Bég, O.A. Numerical study of axisymmetric magneto-gyrotactic bioconvection in non-Fourier tangent hyperbolic nano-functional reactive coating flow of a cylindrical body in porous media, European Physical Journal Plus, 136, 1107 (2021). https://doi.org/10.1140/epjp/s13360-021-02099-z (32 pages)

[9] Morozov, A., and Spagnolie, S.E. Introduction to Complex Fluids, Springer, Biological and Medical Physics, Biomedical Engineering, DOI 10.1007/978 – 1 – 4939 – 2065 – 51

[10] Pleiner, H., Liu, M., and Brand, H.R. Non-Newtonian Constitutive Equations Using the Orientational Order Parameter, Modeling of Soft Matter, 2005, Springer New York, New York, 99 – 109 (2005)

[11] Fetecau, C., and Fetecau, C. Starting solutions for some unsteady unidirectional flows of a second-grade fluid, Int. J. Eng. Sci. 43, 781 – 789 (2005)

[12] Hayat, T., Naeem, I., Ayub, M., Siddiqui, A.M., Asghar, S., and Khalique, C.M. Exact solutions of second grade aligned MHD fluid with prescribed vorticity, Nonlinear Analysis: Real World Appl. 10, 2117 – 2126 (2009)

[13] Fetecau, C., and Fetecau, C. Starting solutions for the motion of a second grade fluid due to longitudnal and torsional oscillations of a circular cylinder, Int. J. Eng. Sci. 44, 788 – 796 (2006)

[14] Tan, W.C., and Masuoka, T. Stokes problem for a second-grade fluid in a porous half space with heated boundary, Int. J. Non-Linear Mech. 40, 515 – 522 (2005)

[15] Asghar, S., Hayat, T., and Ariel, P.D. Unsteady Couette flows in a second-grade fluid with variable material properties, Comm. Nonlinear Sci. Num. Simul. 14, 154 – 159 (2009)

[16] Powell, R.E., and Eyring, H. Nature, London 427, (1944).

[17] Patel, M., and Timol, M.G. Numerical treatment of Powell-Eyring fluid flow using Method of Satisfaction of Asymptotic Boundary Conditions (MSABC), Appl. Num. Math. 59, 2584 − 2592 (2009)

[18] Eldabe, N.T.M., Hassan, A.A., and Mohamed, M.A.A. Effect of couple stresses on the MHD of a non-Newtonian unsteady flow between two parallel porous plates, Z. Naturforsch. 58a, 204 − 210 (2003)

[19] Sakiadis, B.C. Boundary layer behavior on continuous solid surfaces. II: the boundary layer on a continuous flat surface, AIChemE J. 7, 221 − 225 (1961)

[20] Mukhopadhyay, S. Effect of thermal radiation on unsteady mixed convection flow and heat transfer over a stretching surface in a porous medium, Int. J. Heat Mass Transf. 52, 3261 − 3265 (2009)

[21] Hayat, T., Qasim, M., and Abbas, Z. Radiation and mass transfer effects on the magnetohydrodynamic unsteady flow induced by a stretching sheet, Z. Naturforsch A. 65a, 231 − 239 (2010)

[22] Fang, T., Zhang, J., and Yao, S. Slip MHD viscous flow over a stretching sheet: An exact solution, Comm. Nonlinear Sci. Num. Simul. 14, 3731 − 3737 (2009)

[23] Ishak, A., Jafar, K., Nazar, R., and Pop, I. MHD stagnation point flow towards a stretching sheet, Physica A, 388, 3377 − 3383 (2009)

[24] Hayat, T., Iqbal, Z., Mustafa, M., and Obaidat, S. Flow and heat transfer of Jeffrey fluid over a continuously moving surface with a parallel free stream, ASME, J. Heat Transfer, 134(1), 01170 (2011)

[25] Hayat, T., Iqbal, Z., Mustafa, M., and Alsaedi, A. Momentum and heat transfer of an upper-convected Maxwell fluid over a moving surface with convective boundary conditions, Nuclear Engineering and Design, 252, 242 − 247 (2012)

[26] Hayat, T., Iqbal, Z., Qasim, M., and Obaidat, S. Steady flow of an Eyring Powell fluid over a moving surface with convective boundary conditions, Int. J. Heat and Mass Transfer, Int. J. Heat and Mass Transf. 55, 1817 − 1822 (2012)

[27] Zaman, H., Hayat, T., and Ayub, M. Series solution for heat transfer from a continuous surface in a parallel free stream of viscoelastic fluid, Numerical Method for Partial Differential Equations, 27, 1511 − 1524 (2011)

[28] Bég, O.A., Numerical methods for multi-physical magnetohydrodynamics. J.

Magnetohydrodynamics and Plasma Research. 18, 93-200 (2013)

[29] Uddin M.J., Bég, O.A., and Ismail A.I. Radiative-convective nanofluid flow past a stretching/shrinking sheet with slip effects. AIAA J. Thermophysics Heat Transfer, 29, 513-523 (2015)

[30] Sarkar S., and Sahoo B. Oblique stagnation flow towards a rotating disc. European Journal of Mechanics - B/Fluids, 85:82-89 (2021)

[31] Miroslav, P., and Kovalcik A. Effects of thermal annealing as polymer processing step on poly (lactic acid), Materials and Manufacturing Processes, 33, 1674-1680 (2018)

[32] Gaffar, S.A., Bég, O.A., Prasad, V.R., Khan, B.M.H. and Kadir, A. Computation of Eyring-Powell micropolar convective boundary layer flow from an inverted non-isothermal cone: thermal polymer coating simulation, Computational Thermal Sciences, 12(4):329–344 (2020)

[33] Griskey R.G., Mass Transfer in Polymer Systems. In: Polymer Process Engineering. Springer, Dordrecht, Netherlands (1995)